

Energy dissipation and switching delay in spin-transfer torque switching of nanomagnets with low-saturation magnetization in the presence of thermal fluctuations

Kuntal Roy,^{1, a)} Supriyo Bandyopadhyay,¹ Jayasimha Atulasimha,² Kamaram Munira,³ and Avik W. Ghosh³

¹⁾Department of Electrical and Computer Engineering, Virginia Commonwealth University, Richmond, VA 23284, USA

²⁾Department of Mechanical and Nuclear Engineering, Virginia Commonwealth University, Richmond, VA 23284, USA

³⁾Department of Electrical and Computer Engineering, University of Virginia, Charlottesville, VA 22904, USA

(Dated: 16 November 2018)

A common ploy to reduce the switching current and energy dissipation in spin-transfer-torque driven magnetization switching of shape-anisotropic single-domain nanomagnets is to employ magnets with low saturation magnetization M_s and high shape-anisotropy. The high shape-anisotropy compensates for low M_s to keep the static switching error rate constant. However, this ploy increases the switching delay, its variance in the presence of thermal noise, and the dynamic switching error rate. Using the stochastic Landau-Lifshitz-Gilbert equation with a random torque emulating thermal noise, we show that pumping some excess spin-polarized current into the nanomagnet during switching will keep the mean switching delay and its variance constant as we reduce M_s , while still reducing the energy dissipation significantly.

PACS numbers: 75.76.+j, 85.75.Ff, 75.78.Fg, 81.70.Pg

Keywords: Spin-transfer-torque, nanomagnets, LLG equation, thermal analysis

I. INTRODUCTION

Spin-transfer-torque (STT) is an electric current-induced magnetization switching mechanism that can rotate the magnetization axis of a nanomagnet by exerting a torque on it due to the passage of a spin-polarized current¹⁻⁴. The STT-mechanism is routinely used to switch the magnetization of a shape-anisotropic nanomagnet from one stable orientation along the easy axis to the other⁵, and has been demonstrated in numerous experiments involving both spin-valves⁶ and magnetic tunnel junctions (MTJs)⁷. MTJs, consisting of an insulating layer sandwiched between two ferromagnetic layers (one *hard* and the other *soft*), are becoming the staple of *nonvolatile* magnetic random access memory (MRAM)^{8,9} (see Fig. 1). Switching the soft layer of an MTJ with the STT-mechanism (STT-RAM) allows for high integration densities, but usually requires a high current density ($> 10^7$ A/cm²) resulting in significant energy dissipation¹⁰.

One way to decrease energy dissipation in STT-driven switching is to fashion nanomagnets out of materials with low saturation magnetization M_s (e.g., dilute magnetic semiconductors). The spin-polarized switching current I_s , that delivers the spin-transfer-torque and switches the magnetization, varies as M_s^2 (see Refs. [1, 11–13]), so that the power dissipation $I_s^2 R$ (R = resistance of the nanomagnet) should vary as M_s^4 if R does not change. However, reducing M_s decreases the in-plane

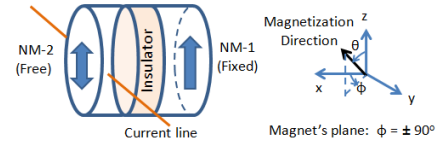


FIG. 1. Simplified schematic diagram of an STT-RAM memory element. The nanomagnets (NMs) are on the y - z plane and are shaped like elliptical cylinders. NM-1 is magnetically hardened along the z -axis so that its magnetization direction is fixed. The magnetization direction of NM-2 can be rotated with an in-plane spin polarized current that delivers a spin-transfer-torque. The magnetization orientation of the free layer NM-2 with respect to the z -axis (0° and 180°) encodes logic bits 0 and 1.

shape anisotropy barrier E_b that separates the two stable magnetization states along the easy axis. This happens because E_b is proportional to the product of M_s^2 and the demagnetization factor of the nanomagnet, which depends on the degree of shape anisotropy. The decrease in E_b increases the probability of random switching between the two stable states, which is $\sim \exp[-E_b/kT]$ ¹⁴⁻¹⁶ at a temperature T . Therefore, if one reduces M_s , then one must also increase the in-plane shape anisotropy (or aspect ratio of the magnet) commensurately in order to keep the barrier E_b and the static error probability unchanged. Increasing the shape anisotropy, or aspect ratio, has another beneficial effect; it decreases the resistance R in the path of the switching current I_s if the latter flows along the in-plane hard axis of the nanomagnet. This further reduces the power dissipation $I_s^2 R$.

It therefore appears that reducing M_s , while increasing

^{a)}Electronic mail: royk@vcu.edu.

shape anisotropy to keep E_b constant, is always beneficial. There is however one caveat. Reducing M_s makes a nanomagnet more vulnerable to thermal fluctuations¹⁷ and can increase both the thermally averaged (mean) switching delay and the standard deviation in the switching delay due to thermal fluctuations. This has a deleterious effect on clock speed and clock synchronization in memory or logic technologies utilizing spin-transfer torque mechanism. Consequently, memory and logic devices utilizing materials with low saturation magnetization often work at low temperatures, even if the Curie temperature of the nanomagnet exceeds room temperature, just so that thermal agitations are suppressed^{18,19}. In this paper, we show that a better approach to contend with thermal fluctuations, when M_s is reduced, is to still work at room temperature, but use slightly more switching current than that required by the $I_s \propto M_s^2$ scaling law. This will decrease the mean switching delay and its variance, while still maintaining a significant energy saving due to the reduced M_s .

II. MODEL

We study the magnetization dynamics of a nanomagnet subjected to a spin-transfer-torque at room temperature by employing the stochastic Landau-Lifshitz-Gilbert (LLG) equation^{20,21}. It describes the time evolution of the magnetization vector in the presence of spin-transfer-torque, the torque due to shape anisotropy, and an additional random torque due to thermal fluctuations. We choose the dimensions of the nanomagnet such that it has always a single ferromagnetic domain²². Thermal effects in magnetization dynamics have been studied both theoretically^{23–28} and experimentally^{29–31}.

We consider a nanomagnet (see Fig. 1) in the shape of an elliptical cylinder whose elliptical cross section lies in the y - z plane with its major axis and minor axis aligned along the z -direction and the y -direction, respectively. The dimension of the major axis is a , that of the minor axis is b , and the thickness is l . The magnet's volume is $\Omega = (\pi/4)abl$. Let $\theta(t)$ be the angle subtended by the magnetization axis with the $+z$ -axis at any instant of time t and $\phi(t)$ be the angle between the $+x$ -axis and the projection of the magnetization axis on the x - y plane. Thus, $\theta(t)$ is the polar angle and $\phi(t)$ is the azimuthal angle. Note that when $\phi = \pm 90^\circ$, the magnetization vector lies in the plane of the nanomagnet.

The potential energy of an isolated unperturbed shape-anisotropic single-domain nanomagnet is the uniaxial shape anisotropy energy given by

$$E_{SHA}(t) = \frac{\mu_0}{2} M_s^2 \Omega N_d(t), \quad (1)$$

where M_s is the saturation magnetization and N_d is the

demagnetization factor expressed as³²

$$N_d(t) = N_{d-zz} \cos^2 \theta(t) + N_{d-yy} \sin^2 \theta(t) \sin^2 \phi(t) + N_{d-xx} \sin^2 \theta(t) \cos^2 \phi(t) \quad (2)$$

with N_{d-zz} , N_{d-yy} , and N_{d-xx} being the components of N_d along the z -axis, y -axis, and x -axis, respectively. The expressions for these quantities can be found in Ref. [33] and they are constrained by the following relation:

$$N_{d-zz} + N_{d-yy} + N_{d-xx} = 1. \quad (3)$$

We have assumed that the use of a properly balanced synthetic antiferromagnetic fixed layer can eliminate the net effect of dipole coupling on the free layer³⁴.

At any instant of time, the total energy of the unperturbed isolated nanomagnet can be expressed as

$$E(t) = E_{SHA}(t) = B(t) \sin^2 \theta(t) + C \quad (4)$$

where

$$B(t) = B(\phi(t)) = \frac{\mu_0}{2} M_s^2 \Omega [N_{d-xx} \cos^2 \phi(t) + N_{d-yy} \sin^2 \phi(t) - N_{d-zz}], \quad (5)$$

$$C = \frac{\mu_0}{2} M_s^2 \Omega N_{d-zz}. \quad (6)$$

The in-plane shape anisotropy energy barrier height (using $\phi = \pm 90^\circ$) can be expressed as

$$E_{SHA, in-plane} = \frac{\mu_0}{2} M_s^2 \Omega N_{d0} \quad (7)$$

where $N_{d0} = [N_{d-yy} - N_{d-zz}]$. Note that the in-plane shape anisotropy energy barrier height is independent of time t even though $E_{SHA}(t)$ is not.

The magnetization $\mathbf{M}(t)$ of the single-domain nanomagnet has a constant magnitude at any given temperature but a variable direction, so that we can represent it by the vector of unit norm $\mathbf{n}_m(t) = \mathbf{M}(t)/|\mathbf{M}| = \hat{\mathbf{e}}_r$ where $\hat{\mathbf{e}}_r$ is the unit vector in the radial direction in spherical coordinate system represented by (r, θ, ϕ) . The other two unit vectors in the spherical coordinate system are denoted by $\hat{\mathbf{e}}_\theta$ and $\hat{\mathbf{e}}_\phi$ for θ and ϕ rotations, respectively. The coordinates (θ, ϕ) completely describe the motion of $\mathbf{M}(t)$ ³.

The torque acting on the magnetization within unit volume due to shape anisotropy is

$$\mathbf{T}_E(t) = -\mathbf{n}_m(t) \times \nabla \mathbf{E}[\theta(t), \phi(t)] = -\{2B(t) \sin \theta(t) \cos \theta(t)\} \hat{\mathbf{e}}_\phi - \{B_{0e}(t) \sin \theta(t)\} \hat{\mathbf{e}}_\theta, \quad (8)$$

where

$$B_{0e}(t) = B_{0e}(\phi(t)) = \frac{\mu_0}{2} M_s^2 \Omega (N_{d-xx} - N_{d-yy}) \sin(2\phi(t)). \quad (9)$$

Passage of a constant spin-polarized current I_s through the nanomagnet generates a spin-transfer-torque that is given by³

$$\mathbf{T}_{STT}(t) = s \sin \theta(t) \hat{\mathbf{e}}_\theta, \quad (10)$$

where $s = (\hbar/2e)\eta I_s$ is the spin angular momentum deposition per unit time and η is the degree of spin-polarization in the current I_s .

The effect of thermal fluctuations is to produce a *random* magnetic field $\mathbf{h}(t)$ expressed as

$$\mathbf{h}(t) = h_x(t) \hat{\mathbf{e}}_x + h_y(t) \hat{\mathbf{e}}_y + h_z(t) \hat{\mathbf{e}}_z \quad (11)$$

where $h_x(t)$, $h_y(t)$, and $h_z(t)$ are the three components in x -, y -, and z -direction, respectively. We will assume the same properties of the random field $\mathbf{h}(t)$ as described in the Ref. [35]. Accordingly, the random thermal field can be expressed as³⁶

$$h_i(t) = \sqrt{\frac{2\alpha kT}{|\gamma|(1+\alpha^2)M_V\Delta t}} G_{(0,1)}(t) \quad (i = x, y, z) \quad (12)$$

where α is the dimensionless phenomenological Gilbert damping constant, $\gamma = 2\mu_B\mu_0/\hbar$ is the gyromagnetic ratio for electrons and is equal to 2.21×10^5 (rad.m).(A.s)⁻¹, μ_B is the Bohr magneton, $M_V = \mu_0 M_s \Omega$, $1/\Delta t$ is the attempt frequency of the random thermal field affecting the magnetization dynamics; therefore Δt should be chosen as the simulation time-step used to solve the coupled LLG equations numerically, and $G_{(0,1)}(t)$ is a Gaussian distribution with zero mean and unit standard deviation. Note that the variance in the random thermal fields is inversely proportional to the saturation magnetization M_s ; therefore a lower saturation magnetization augments the detrimental effects of thermal fluctuations.

The thermal torque can be written as

$$\mathbf{T}_{\text{TH}}(t) = M_V \mathbf{n}_m(t) \times \mathbf{h}(t) = P_\theta(t) \hat{\mathbf{e}}_\phi - P_\phi(t) \hat{\mathbf{e}}_\theta \quad (13)$$

where

$$P_\theta(t) = M_V [h_x(t) \cos\theta(t) \cos\phi(t) + h_y(t) \cos\theta(t) \sin\phi(t) - h_z(t) \sin\theta(t)], \quad (14)$$

$$P_\phi(t) = M_V [h_y(t) \cos\phi(t) - h_x(t) \sin\phi(t)]. \quad (15)$$

The magnetization dynamics of the single-domain nanomagnet under the action of various torques is described by the stochastic Landau-Lifshitz-Gilbert (LLG) equation as

$$\begin{aligned} \frac{d\mathbf{n}_m(t)}{dt} - \alpha \left(\mathbf{n}_m(t) \times \frac{d\mathbf{n}_m(t)}{dt} \right) \\ = -\frac{|\gamma|}{M_V} [\mathbf{T}_E(t) + \mathbf{T}_{\text{STT}}(t) + \mathbf{T}_{\text{TH}}(t)]. \end{aligned} \quad (16)$$

In spherical coordinate system, with constant magnitude of magnetization, we get the following coupled equations for θ - and ϕ -dynamics.

$$\begin{aligned} (1 + \alpha^2) \theta'(t) = \frac{|\gamma|}{M_V} [(B_{0e}(t) - s) \sin\theta(t) \\ - 2\alpha B(t) \sin\theta(t) \cos\theta(t) + (\alpha P_\theta(t) + P_\phi(t))] \end{aligned} \quad (17)$$

$$\begin{aligned} (1 + \alpha^2) \phi'(t) = \frac{|\gamma|}{M_V} [\alpha(B_{0e}(t) - s) \\ + 2B(t) \cos\theta(t) - [\sin\theta(t)]^{-1} (P_\theta(t) - \alpha P_\phi(t))]. \end{aligned} \quad (18)$$

The application of an in-plane spin-polarized current I_s to produce spin-transfer torque results in an energy dissipation $I_s^2 R \tau$, where R is the in-plane resistance of the elliptical cylinder given by $R = \rho(2/\pi)(b/a)l$ with ρ being the resistivity of the material used and τ is the switching delay.

Furthermore, because of Gilbert damping in the nanomagnet, an additional energy E_d is dissipated when the magnetization axis in the nanomagnet switches from one orientation to the other along the easy axis. This energy is given by the expression $E_d = \int_0^\tau P_d(t) dt$, where τ is the *switching delay* and $P_d(t)$ is the dissipated power given by^{37,38}

$$P_d(t) = \frac{\alpha |\gamma|}{(1 + \alpha^2) M_V} |\mathbf{T}_E(t) + \mathbf{T}_{\text{STT}}(t)|^2. \quad (19)$$

Thermal torque does not cause any net energy dissipation since mean of the thermal field is zero.

The thermal distributions of θ and ϕ in an unperturbed magnet are found by solving the Equations (17) and (18) while setting $I_s = 0$. This will yield the distribution of the magnetization vector's initial orientation ($\theta_{init}, \phi_{init}$) when stress is turned on. We consider magnetization initially situated at $\theta = 180^\circ$. The θ -distribution is Boltzmann peaked at $\theta = 180^\circ$ with mean $\sim 175.5^\circ$, while the ϕ -distribution is Gaussian peaked at $\phi = \pm 90^\circ$ ³⁹.

The quantity τ for any switching trajectory is determined by solving the coupled equations (17) and (18) starting with an initial orientation ($\theta_{init}, \phi_{init}$) and terminating the trajectory when $\theta(t)$ reaches a pre-defined θ_{final} , regardless of what the corresponding ϕ_{final} is. The time taken for a trajectory to complete (i.e., for $\theta(t)$ to reach θ_{final}) is the value of τ for that trajectory. The average value $\langle \tau \rangle$ and the standard deviation $\langle \Delta \tau \rangle$ are found by simulating numerous (10,000) trajectories in the presence of the random thermal torque, and then extracting these quantities from the distribution.

The total energy E_{total} dissipated in completing any trajectory is given by $E_{total} = E_d + I_s^2 R \tau$. The average power dissipated in completing any trajectory is simply E_{total}/τ . We can find the thermal average of E_d and its variance by calculating E_d for numerous trajectories and then computing these quantities from the distribution.

III. SIMULATION RESULTS

We consider a nanomagnet made of CoFeB alloy which has low saturation magnetization¹² and a low Gilbert damping factor of $\alpha = 0.01$. The saturation magnetization can be varied by varying the alloy composition¹². The resistivity is assumed to be the same as that of cobalt, i.e. $\rho = 5.81 \times 10^{-8} \Omega\text{-m}$ [Ref. 40]. We choose this material over dilute magnetic semiconductors which have

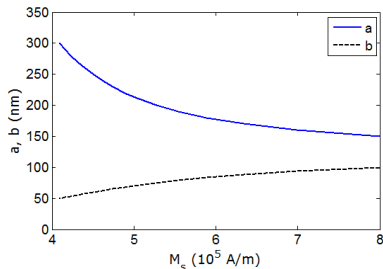


FIG. 2. Variation of the major axis (a) and the minor axis (b) with the saturation magnetization (M_s) needed to maintain a constant in-plane shape anisotropy barrier of 0.8 eV or ~ 32 kT at room temperature. The thickness of the nanomagnet is held constant at $l = 2$ nm.

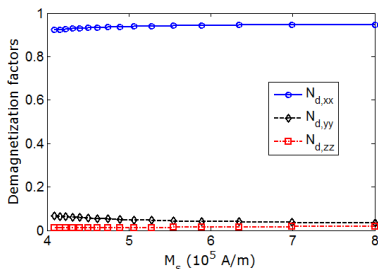


FIG. 3. Demagnetization factors needed for different values of saturation magnetization M_s in order to keep the in-plane shape anisotropy barrier constant at 0.8 eV or ~ 32 kT at room temperature. The demagnetization factors are computed from the major and minor axes values in Fig. 2 and with constant thickness of 2 nm.

much smaller M_s because the latter's M_s is so small^{18,19} that it will be impossible to make the in-plane shape anisotropy barrier E_b (which is proportional to $M_s^2 \Omega N_{d0}$) large enough (32 kT or 0.8 eV) without making the volume Ω of the nanomagnet very large. With that large volume, the nanomagnet will no longer be single-domain. Choosing CoFeB allows us to work at room temperature with a barrier of 0.8 eV or ~ 32 kT , while still ensuring single-domain behavior because the volume can be kept small.

In order to maintain a constant value of $E_b = 0.8$ eV as we vary M_s , we increase the shape anisotropy of the nanomagnet (or the aspect ratio a/b of the ellipse) to increase N_{d0} and compensate for any decrease in M_s . As we vary the aspect ratio a/b , we keep the cross-sectional area of the ellipse $[(\pi/4)ab]$ and the thickness l constant, which keeps both the area and the volume of the nanomagnet Ω constant. The rationale behind keeping the cross-sectional area of the nanomagnet constant is to keep the density of devices per unit area on the chip constant.

The in-plane shape anisotropy energy barrier depends on three quantities: M_s , N_{d0} and Ω [see Equation (7)]. Since we keep Ω constant, we compensate for any decrease in M_s by commensurately increasing N_{d0} alone. At all times, we ensure that the dimensions chosen (a ,

b , and l) guarantee that the nanomagnet remains in the single-domain limit^{22,33}. The thickness l is held constant at 2 nm.

Fig. 2 shows how the major axis a and the minor axis b should vary with M_s to keep the in-plane shape anisotropy energy barrier constant at 0.8 eV. This ensures that the *static* error probability associated with spontaneous switching between the two stable states along the easy axis remains constant as we vary M_s and N_{d0} . In Fig. 3, we plot the three components of demagnetization factor for different values of M_s that will keep the in-plane shape anisotropy barrier constant at 0.8 eV. Obviously, as M_s is decreased, we need to increase the value of N_{d0} , i.e. $(N_{d-yy} - N_{d-zz})$, to keep the same in-plane shape anisotropy energy barrier height. With decreasing M_s , the quantity N_{d-yy} increases significantly while N_{d-zz} remains more or less constant. Since the three components of the demagnetization factor are constrained by the relation $N_{d-xx} + N_{d-yy} + N_{d-zz} = 1$, the value of N_{d-xx} must decrease proportionately, which is seen in Fig. 3.

A. Dependence of switching delay and energy dissipation on saturation magnetization

We assume that when a spin-polarized current is applied to initiate switching, the magnetization vector starts out from near the south pole ($\theta \simeq 180^\circ$) with a certain $(\theta_{init}, \phi_{init})$ picked from the initial angle distributions at 300 K³⁹. The magnetization dynamics ensures that θ continues to rotate towards 0° , while temporary backtracking of θ may occur due to random thermal kicks. Thermal fluctuations can introduce a spread in the time it takes to reach $\theta \simeq 0^\circ$ but cannot prevent magnetization to reach $\theta \simeq 0^\circ$. When θ becomes $\leq 4.5^\circ$, switching is deemed to have completed. A moderately large number (10,000) of simulations, with their corresponding $(\theta_{init}, \phi_{init})$ picked from the initial angle distributions, are performed for each value of saturation magnetization to generate the simulation results in this subsection. The magnitude of the switching current I_s is 2 mA at $M_s = 8 \times 10^5$ A/m and it is reduced proportionately with the square of M_s for other values of M_s . The spin polarization of the current is always 80%.

Figs. 4 and 5 show the mean switching delay and the mean energy dissipation for different values of saturation magnetization M_s when the in-plane shape anisotropy energy barrier is held constant at 0.8 eV by adjusting the nanomagnet's shape (and thus demagnetization factors) as we vary M_s . In generating these plots, the magnitude of the in-plane spin-polarized current is chosen as 2 mA when $M_s = 8 \times 10^5$ A/m and the switching current I_s was decreased in accordance with the $I_s \propto M_s^2$ scaling law. Each scattered point (denoted 'single run') in the figure is the switching delay for *one* representative switching trajectory at that value of M_s . There is considerable scatter in the 'single run' data which is significantly reduced by

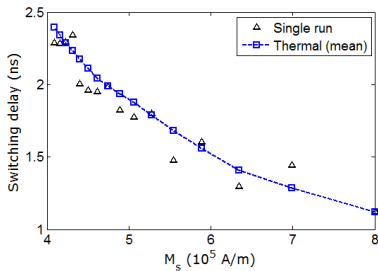


FIG. 4. Switching delay τ at room temperature (300 K) in a nanomagnet of fixed in-plane shape anisotropy energy barrier of 0.8 eV as a function of saturation magnetization M_s . Switching current I_s is 2 mA at $M_s = 8 \times 10^5$ A/m and it is reduced proportionately with the square of M_s for other values of M_s . The spin polarization of the current is always 80%.

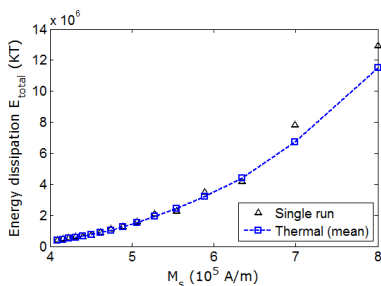


FIG. 5. Total energy dissipation in a nanomagnet of fixed in-plane shape anisotropy energy barrier of 0.8 eV as a function of saturation magnetization M_s at room temperature (300 K). The total dissipation includes the dissipation in the switching circuit $I_s^2 R \tau$ and the internal energy dissipation E_d . The internal energy dissipation E_d is only a very small fraction of the total energy dissipation E_{total} .

thermal averaging (averaging over many trajectories).

The *large* scatter in the ‘single run’ data points is not caused by the random thermal torque since we get the similar trend without incorporating thermal fluctuations. The scatter is more prominent at smaller values of M_s , which corresponds to lower I_s ($I_s \propto M_s^2$). At lower I_s , the magnetization dynamics is more complex since there are more ripples (see Fig. 8 and Fig. 9 later). As a result, there is more variability in the switching dynamics (and hence switching delay) with changing I_s when the latter is small. This variability contributes to the scatter.

In Fig. 4, we find that the mean switching delay $\langle \tau \rangle$ decreases with increasing saturation magnetization M_s . This can be explained as follows. The spin-transfer torque is proportional to I_s/M_s . Since $I_s \propto M_s^2$, the spin-transfer-torque becomes proportional to M_s . Therefore, reducing M_s weakens the spin-transfer-torque. Since the in-plane shape anisotropy energy barrier is invariant, it takes longer for the weakened spin-transfer torque to overcome the in-plane shape anisotropy barrier and cause switching. This makes switching delay increase with decreasing M_s .

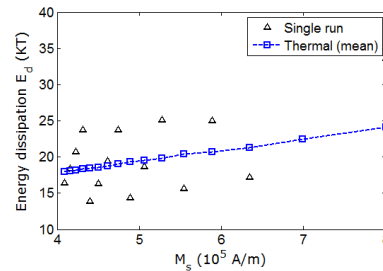


FIG. 6. Internal energy dissipation E_d for different values of saturation magnetization at 300 K. This energy dissipation is several orders of magnitude smaller than the energy dissipation in the external circuitry thus it is only a very small fraction of the total energy dissipation E_{total} .

In Fig. 5, we plot the thermal means of the energy dissipation E_{total} at 300 K as a function of the saturation magnetization M_s , while keeping the in-plane shape anisotropy barrier constant. E_{total} is overwhelmingly dominated by the component $I_s^2 R \tau$, and the internal energy dissipation E_d has a minor contribution [see Fig. 6]. The switching current I_s varies as the square of M_s , so that I_s^2 varies as M_s^4 . Furthermore, if we reduce M_s , we have to increase the shape anisotropy (or the aspect ratio a/b) to keep the in-plane shape anisotropy energy barrier constant. If the switching current flows along the minor axis of the elliptical nanomagnet (always preferable since it results in minimum resistance in the path of the current), then increasing the ratio a/b decreases the nanomagnet’s electrical resistance proportionately. Thus, both I_s and R will decrease with decreasing M_s (the latter because the in-plane shape anisotropy barrier is kept constant). Consequently, the *power* dissipation $I_s^2 R$ increases with M_s more rapidly than M_s^4 . Unless the switching delay τ has a stronger dependence on M_s than $\tau \propto M_s^{-4}$, we will expect the energy dissipation to decrease with decreasing M_s and that is precisely what we observe in Fig. 5.

The last two figures highlight two important facts: (1) the energy dissipated to switch can be reduced by decreasing M_s while maintaining a fixed in-plane shape anisotropy energy barrier to keep the *static* error probability fixed, and (2) the switching delay increases if we reduce M_s while keeping the in-plane shape anisotropy energy barrier fixed. Thus, there are *two* penalties involved with reducing energy dissipation by lowering M_s and scaling I_s quadratically with M_s : (i) slower switching, and (ii) higher *dynamic* error probability due to an increased variance in thermal field [see Equation (12)].

For the nanomagnet that we have considered (with the parameters described earlier), we find that lowering the saturation magnetization M_s by a factor of ~ 2 decreases the energy dissipation by ~ 28 times while increasing the switching delay by approximately *twice*. The factor of ~ 2 decrease in M_s causes a ~ 16 -fold decrease in I_s^2 (since $I_s \propto M_s^2$). Additionally, there is ~ 4 -fold decrease in

the resistance of the nanomagnet owing to the fact that the shape anisotropy is increased to keep the in-plane shape anisotropy energy barrier constant. Thus, the ~ 64 -fold decrease in power dissipation and the 2-fold increase in switching delay together cause a net decrease of ~ 28 times in the total energy dissipation. Therefore, if we decrease the saturation magnetization by a factor of ~ 2 , then we will: (1) gain 28-fold in energy dissipation; (2) lose 2-fold in switching speed; and (3) lose somewhat in error rates due to thermal agitation since the variance in switching delay is increased.

B. Constant switching delay scaling

In order to understand how we can maintain a constant switching delay while scaling M_s , let us consider the relationship between switching current and switching delay. In Figs. 7 and 8, we plot the magnetization dynamics without considering any thermal fluctuations during the switching when $M_s = 8 \times 10^5$ A/m and $M_s = 4.09 \times 10^5$ A/m, respectively. The switching current has been decreased from 2 mA for $M_s = 8 \times 10^5$ A/m to 523 μ A for $M_s = 4.09 \times 10^5$ A/m, in accordance with the square-law scaling $I_s \propto M_s^2$. In Figs. 7 and 8, we have assumed the same initial orientation of magnetization $\theta_{init} = 175.5^\circ$ and $\phi_{init} = 90^\circ$, which are thermally mean values for 300 K to avoid the stagnation point exactly along the easy axis. The square-law scaling however results in an increased switching delay since the latter has obviously increased by a factor of 2 (from 1.05 ns to 2.1 ns). This has happened because of more ripples generating from more precessional motion of the magnetization vector seen in Fig. 8. In order to maintain the same switching delay of 1.05 ns as before, we will have to deviate from the square-law scaling and increase the switching current by nearly two times to 1.05 mA. Thus, we need to pump an excess current of 1.05 mA - 0.523 mA = 0.527 mA in order to maintain the same switching speed. The corresponding magnetization dynamics without considering any thermal fluctuations during the switching is shown in Fig. 9, where we have clearly recovered the 1.05 ns delay. The energy dissipation (dominated by $I_s^2 R \tau$) now goes up by a factor of two [I_s increases by a factor of two while τ decreases by a factor of two]. Thus, we find that if we wish to maintain a *constant switching delay*, then we need to inject some excess current over that dictated by square-law scaling and therefore suffer some excess energy dissipation. This excess energy dissipation is sufficiently small so that there is still considerable energy saving accruing from the reduction in M_s . Reducing M_s by a factor of ~ 2 results in a net energy saving of ~ 14 times, instead of the ~ 28 times estimated without imposing the requirement of constant switching delay. The important point is that *we have extracted a very significant energy saving by reducing M_s by a factor of 2, without sacrificing switching speed.*

For illustrative purposes, we show in Fig. 10 the mag-

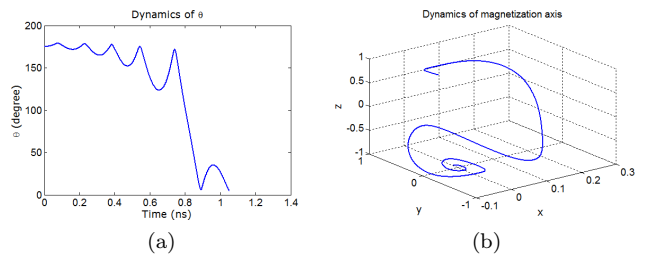


FIG. 7. Switching dynamics of the magnetization vector in a nanomagnet of major axis $a = 150$ nm, minor axis $b = 100$ nm, and $M_s = 8 \times 10^5$ A/m, and in-plane shape anisotropy energy barrier of 0.8 eV. This simulation does not consider any thermal fluctuations during the switching, however, the initial orientation of the magnetization is assumed to be $\theta_{init} = 175.5^\circ$ and $\phi_{init} = 90^\circ$ (thermally mean values for 300 K) to avoid the stagnation point exactly along the easy axis. Switching is caused by spin-transfer torque induced with an in-plane current of 2 mA with 80% spin polarization. (a) polar angle $\theta(t)$ versus time, and (b) the trajectory traced out by the tip of the magnetization vector during switching. Switching delay and energy dissipation are 1.05 ns and 1.25×10^7 kT [at room temperature], respectively.

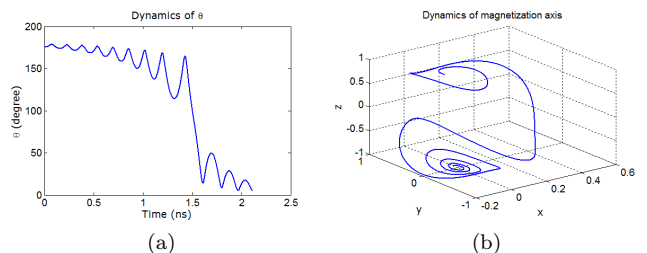


FIG. 8. Switching dynamics for $M_s = 4.09 \times 10^5$ A/m and spin-transfer torque switching current I_s of 523 μ A with 80% spin polarization. This simulation does not consider any thermal fluctuations during the switching, however, the initial orientation of the magnetization is assumed to be $\theta_{init} = 175.5^\circ$ and $\phi_{init} = 90^\circ$ (thermally mean values for 300 K) to avoid the stagnation point exactly along the easy axis. (a) Polar angle $\theta(t)$ versus time, and (b) the trajectory traced out by the tip of the magnetization vector while switching occurs. The switching delay and the energy dissipation are 2.1 ns and 4.3×10^5 kT [at room temperature], respectively.

netization dynamics in the presence of thermal fluctuations at 300 K for the same parameters as in Fig. 9. This is one representative run picked out from 10,000 simulations of the switching trajectory. Note that there is only some quantitative difference, but not much qualitative difference, between Figs. 9 and 10. The ripples are somewhat larger in amplitude and the precessional motion is slightly exacerbated. The switching delay has increased by $\sim 12\%$ in the presence of thermal agitations, however, it should be pointed out that the switching delay may decrease as well when the net effect of thermal agitations aids the magnetization rotation.

Fig. 11 shows how the standard deviations in switching delay and energy dissipation due to thermal fluctu-

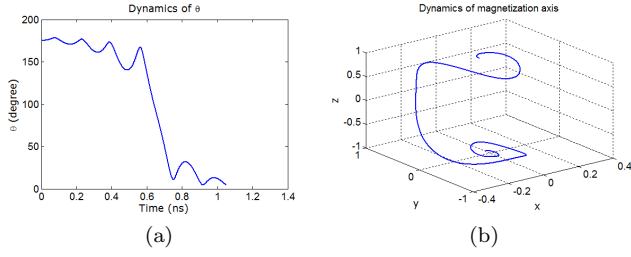


FIG. 9. Switching dynamics for $M_s = 4.09 \times 10^5$ A/m and spin-transfer torque switching current I_s of 1.05 mA with 80% spin polarization. This simulation does not consider any thermal fluctuations during the switching, however, the initial orientation of the magnetization is assumed to be $\theta_{init} = 175.5^\circ$ and $\phi_{init} = 90^\circ$ (thermally mean values for 300 K) to avoid the stagnation point exactly along the easy axis. (a) Polar angle $\theta(t)$ versus time, and (b) the trajectory traced out by the tip of the magnetization vector while switching occurs. The switching delay and the energy dissipation are 1.05 ns and 8.6×10^5 kT [at room temperature], respectively.

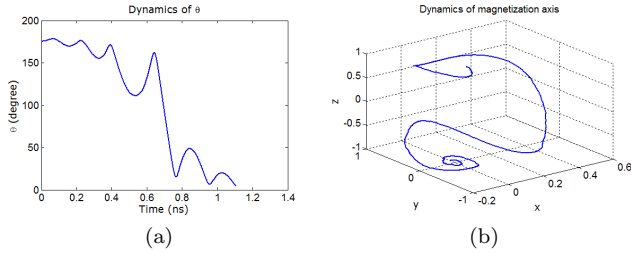


FIG. 10. Switching dynamics at 300 K for $M_s = 4.09 \times 10^5$ A/m and spin-transfer torque switching current I_s of 1.05 mA with 80% spin polarization. The initial orientation of the magnetization is $\theta_{init} = 175.5^\circ$ and $\phi_{init} = 90^\circ$, which are the thermal mean values. This is one specific run from 10,000 MC simulations. (a) Polar angle $\theta(t)$ versus time, and (b) the trajectory traced out by the tip of the magnetization vector while switching occurs. The switching delay and the energy dissipation are 1.18 ns and 9.6×10^5 kT [at room temperature], respectively.

ations depend on the saturation magnetization M_s . As expected, the standard deviation in switching delay increases with decreasing M_s , because the random thermal fields $h_i(t)$ ($i=x,y,z$), which are responsible for the standard deviation, has a $1/\sqrt{M_s}$ dependence [see Equation (12)]. Furthermore, if we scale I_s as M_s^2 , then the spin-transfer torque also decreases as we reduce M_s and that makes the increased thermal field even more effective in randomizing the switching delay. For this reason, the error probability (or switching failure rate) increases when M_s decreases. This problem too can be overcome with some excess switching current. Our simulations have shown that if we increase the switching current from 523 μ A to 1.05 mA, while holding M_s constant at 4.09×10^5 A/m, then the standard deviation in the switching delay goes down from 0.48 ns to 0.23 ns. Note that in this way we have recovered approximately

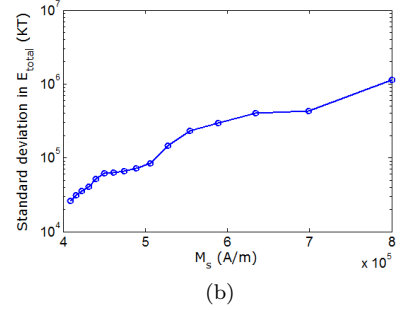
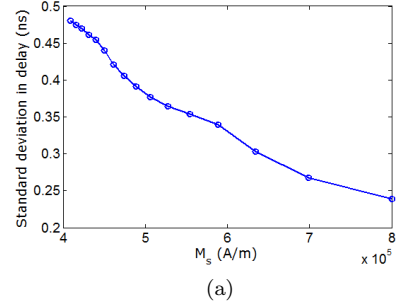


FIG. 11. Standard deviation in switching delay and energy dissipation due to thermal fluctuations at 300 K as a function of saturation magnetization M_s in a nanomagnet with fixed in-plane shape anisotropy energy barrier of 0.8 eV. (a) Standard deviation in switching delay. (b) Standard deviation in energy dissipation.

the same standard deviation in switching delay as that for $M_s = 8 \times 10^5$ A/m.

The standard deviation in energy dissipation however shows the opposite trend, i.e. it decreases with decreasing M_s . This happens because the energy dissipation E_{total} is dominated by $I_s^2 R \tau$, which is proportional to $M_s^4 R \tau$. Lowering M_s increases the standard deviation in τ , but that increase is more than offset by the lower value of M_s , so that the net standard deviation in $I_s^2 R \tau$ actually decreases with decreasing M_s . The excess current that we pump now has a deleterious effect. If we increase the switching current from 523 μ A to 1.05 mA while holding M_s constant at 4.09×10^5 A/m, then the standard deviation in energy dissipation goes up from 2.6×10^4 kT to 9.2×10^4 kT.

The ratio of the standard deviation to the mean is relatively independent of M_s for both the switching delay and the total energy dissipation at 300 K. This ratio does not vary by more than 5% when M_s is varied between 4.09×10^5 and 8×10^5 A/m.

IV. DISCUSSIONS AND CONCLUSIONS

We have shown that one can significantly reduce energy dissipation in spin-transfer torque driven switching of shape-anisotropic nanomagnets by reducing the saturation magnetization of the magnet with appropriate

material choice, while maintaining a constant in-plane shape anisotropy energy barrier (by increasing the magnet's aspect ratio) and a constant mean switching speed (by pumping some excess current) in the presence of thermal fluctuations. Also, the increased variance in switching delay due to lower saturation magnetization can be mitigated by pumping some excess current. In the end, by employing these strategies, one can make the energy dissipation in spin-transfer torque driven switching of nanomagnets competitive with other technologies, without sacrificing switching speed. This bodes well for applications of spin-transfer torque switched nanomagnets in non-volatile logic and memory.

- ¹J. C. Slonczewski, *J. Magn. Magn. Mater.* **159**, L1 (1996).
- ²L. Berger, *Phys. Rev. B* **54**, 9353 (1996).
- ³J. Z. Sun, *Phys. Rev. B* **62**, 570 (2000).
- ⁴J. Z. Sun, *IBM J. Res. Dev.* **50**, 81 (2006).
- ⁵W. J. Gallagher and S. S. P. Parkin, *IBM J. Res. Dev.* **50**, 5 (2006).
- ⁶J. A. Katine, F. J. Albert, R. A. Buhrman, E. B. Myers, and D. C. Ralph, *Phys. Rev. Lett.* **84**, 3149 (2000).
- ⁷G. D. Fuchs, J. A. Katine, S. I. Kiselev, D. Mauri, K. S. Wooley, D. C. Ralph, and R. A. Buhrman, *Phys. Rev. Lett.* **96**, 186603 (2006).
- ⁸S. S. P. Parkin, K. P. Roche, M. G. Samant, P. M. Rice, R. B. Beyers, R. E. Scheuerlein, E. J. O'Sullivan, S. L. Brown, J. Buchigano, and D. W. Abraham, *J. Appl. Phys.* **85**, 5828 (1999).
- ⁹C. Chappert, A. Fert, and F. N. V. Dau, *Nature Mater.* **6**, 813 (2007).
- ¹⁰K. Roy, S. Bandyopadhyay, and J. Atulasimha, *Appl. Phys. Lett.* **99**, 063108 (2011).
- ¹¹E. B. Myers, D. C. Ralph, J. A. Katine, R. N. Louie, and R. A. Buhrman, *Science* **285**, 867 (1999).
- ¹²K. Yagami, A. A. Tulapurkar, A. Fukushima, and Y. Suzuki, *Appl. Phys. Lett.* **85**, 5634 (2004).
- ¹³H. Kubota, A. Fukushima, K. Yakushiji, S. Yakata, S. Yuasa, K. Ando, M. Ogane, Y. Ando, and T. Miyazaki, *J. Appl. Phys.* **105**, 07D117 (2009).
- ¹⁴R. Landauer and J. A. Swanson, *Phys. Rev.* **121**, 1668 (1961).
- ¹⁵R. Landauer, *IBM J. Res. Dev.* **5**, 183 (1961).
- ¹⁶K. K. Likharev, *Int. J. Theor. Phys.* **21**, 311 (1982).
- ¹⁷V. Skumryev, S. Stoyanov, Y. Zhang, G. Hadjipanayis, D. Givord, and J. Nogus, *Nature* **423**, 850 (2003).
- ¹⁸H. Ohno, A. Shen, F. Matsukura, A. Oiwa, A. Endo, S. Katsumoto, and Y. Iye, *Appl. Phys. Lett.* **69**, 363 (1996).
- ¹⁹S. Mark, P. Durrenfeld, K. Pappert, L. Ebel, K. Brunner, C. Gould, and L. W. Molenkamp, *Phys. Rev. Lett.* **106**, 57204 (2011).
- ²⁰L. Landau and E. Lifshitz, *Phys. Z. Sowjet.* **8**, 101 (1935).
- ²¹T. L. Gilbert, *IEEE Trans. Magn.* **40**, 3443 (2004).
- ²²R. P. Cowburn, D. K. Koltsov, A. O. Adeyeye, M. E. Welland, and D. M. Tricker, *Phys. Rev. Lett.* **83**, 1042 (1999).
- ²³J. Fidler and T. Schrefl, *J. Phys. D: Appl. Phys.* **33**, R135 (2000).
- ²⁴D. M. Apalkov and P. B. Visscher, *Phys. Rev. B* **72**, 180405 (2005).
- ²⁵Z. Li and S. Zhang, *Phys. Rev. B* **69**, 134416 (2004).
- ²⁶J. He, J. Z. Sun, and S. Zhang, *J. Appl. Phys.* **101**, 09A501 (2007).
- ²⁷X. Wang, Y. Zheng, H. Xi, and D. Dimitrov, *J. Appl. Phys.* **103**, 034507 (2008).
- ²⁸X. Z. Cheng, M. B. A. Jalil, H. K. Lee, and Y. Okabe, *Phys. Rev. Lett.* **96**, 67208 (2006).
- ²⁹R. H. Koch, J. A. Katine, and J. Z. Sun, *Phys. Rev. Lett.* **92**, 88302 (2004).
- ³⁰E. B. Myers, F. J. Albert, J. C. Sankey, E. Bonet, R. A. Buhrman, and D. C. Ralph, *Phys. Rev. Lett.* **89**, 196801 (2002).
- ³¹D. Bedau, H. Liu, J. Z. Sun, J. A. Katine, E. E. Fullerton, S. Mangin, and A. D. Kent, *Appl. Phys. Lett.* **97**, 262502 (2010).
- ³²S. Chikazumi, *Physics of Magnetism* (Wiley New York, 1964).
- ³³M. Beleggia, M. D. Graef, Y. T. Millev, D. A. Goode, and G. E. Rowlands, *J. Phys. D: Appl. Phys.* **38**, 3333 (2005).
- ³⁴L. Liu, T. Moriyama, D. C. Ralph, and R. A. Buhrman, *Appl. Phys. Lett.* **94**, 122508 (2009).
- ³⁵W. F. Brown, *Phys. Rev.* **130**, 1677 (1963).
- ³⁶B. Behin-Aein, D. Datta, S. Salahuddin, and S. Datta, *Nature Nanotechnol.* **5**, 266 (2010).
- ³⁷Z. Z. Sun and X. R. Wang, *Phys. Rev. B* **71**, 174430 (2005).
- ³⁸B. Behin-Aein, S. Salahuddin, and S. Datta, *IEEE Trans. Nanotech.* **8**, 505 (2009).
- ³⁹See supplementary material at for detailed derivations and additional simulation results.
- ⁴⁰<http://www.allmeasures.com/Formulae/static/materials/>.

Supplementary Information

Energy dissipation and switching delay in spin-transfer torque switching of nanomagnets with low-saturation magnetization in the presence of thermal fluctuations

Kuntal Roy¹, Supriyo Bandyopadhyay¹, and Jayasimha Atulasimha²
 Email: {royk, sbandy, jatulasimha}@vcu.edu

¹Electrical and Computer Engg., Virginia Commonwealth University, Richmond, VA 23284

²Mechanical and Nuclear Engg., Virginia Commonwealth University, Richmond, VA 23284

November 16, 2018

In this supplementary section, we provide further details of the analysis and some additional results.

Contents

S1 Fluctuation about the easy axis due to thermal torque	1
S2 Thermal distributions for θ_{init} and ϕ_{init}	2
S3 Distributions of switching delay and energy dissipation in the presence of thermal fluctuations	4
S4 The benefits of switching with a larger switching current I_s	4
S5 Switching delay-energy as a function of M_s	7

S1 Fluctuation about the easy axis due to thermal torque

We here explicitly show that thermal fluctuations by themselves can dislodge the magnetization from the easy axis. At $T = 0$ K, $\theta_{init} = 180^\circ$. In this case, spin-transfer-torque can never budge the magnetization vector since it vanishes whenever $\sin\theta = 0$. However, when $T > 0$ K, thermal fluctuations can dislodge the magnetization from the easy axis.

In the spherical coordinate system, with constant magnitude of magnetization

$$\frac{d\mathbf{n}_m(t)}{dt} = \frac{d\theta(t)}{dt} \hat{\mathbf{e}}_\theta + \sin\theta(t) \frac{d\phi(t)}{dt} \hat{\mathbf{e}}_\phi. \quad (\text{S1})$$

Accordingly,

$$\alpha \left(\mathbf{n}_m(t) \times \frac{d\mathbf{n}_m(t)}{dt} \right) = -\alpha \sin\theta(t) \phi'(t) \hat{\mathbf{e}}_\theta + \alpha \theta'(t) \hat{\mathbf{e}}_\phi \quad (\text{S2})$$

and

$$\frac{d\mathbf{n}_m(t)}{dt} - \alpha \left(\mathbf{n}_m(t) \times \frac{d\mathbf{n}_m(t)}{dt} \right) = [\theta'(t) + \alpha \sin\theta(t) \phi'(t)] \hat{\mathbf{e}}_\theta + [\sin\theta(t) \phi'(t) - \alpha \theta'(t)] \hat{\mathbf{e}}_\phi \quad (\text{S3})$$

where $()'$ denotes $d()/dt$. Equating the \hat{e}_θ and \hat{e}_ϕ components of the LLG equation [Equation (16) in the main paper] and using Equations (8) and (10) in the main paper, we get

$$\theta'(t) + \alpha \sin\theta(t) \phi'(t) = \frac{|\gamma|}{M_V} [B_{0e}(t) \sin\theta(t) - s \sin\theta(t) + P_\phi(t)] \quad (\text{S4})$$

$$\sin\theta(t) \phi'(t) - \alpha\theta'(t) = \frac{|\gamma|}{M_V} [2B(t) \sin\theta(t) \cos\theta(t) + s \sin\theta(t) - P_\theta(t)]. \quad (\text{S5})$$

When $\sin\theta = 0$, Equations (S4) and (S5) yield

$$\theta'(t) = \frac{|\gamma|}{M_V} P_\phi(t) \quad (\text{S6})$$

$$\alpha\theta'(t) = \frac{|\gamma|}{M_V} P_\theta(t). \quad (\text{S7})$$

Substituting for $P_\theta(t)$ and $P_\phi(t)$ from Equations (14) and (15) as in the main paper and using $\theta = 180^\circ$, we get

$$\alpha h_x(t) \sin\phi(t) - \alpha h_y(t) \cos\phi(t) = h_x(t) \cos\phi(t) + h_y(t) \sin\phi(t) \quad (\text{S8})$$

which yields

$$\phi(t) = \tan^{-1} \left(\frac{\alpha h_y(t) + h_x(t)}{\alpha h_x(t) - h_y(t)} \right). \quad (\text{S9})$$

Using this value of $\phi(t)$ in either Equation (S6) or Equation (S7), we get

$$\theta'(t) = -|\gamma| \frac{h_x^2(t) + h_y^2(t)}{\sqrt{(\alpha h_y(t) + h_x(t))^2 + (\alpha h_x(t) - h_y(t))^2}}. \quad (\text{S10})$$

We can see from the above equation that thermal torque can dislodge the magnetization vector from the easy axis because the time rate of change of $\theta(t)$, i.e. $\theta'(t)$, is non-zero, even though $\sin\theta = 0$. Note that the initial rate of deflection of the magnetization vector from the easy axis does not depend on the component of the random magnetic field along the z -axis [$h_z(t)$], which is a consequence of having the z -axis as the easy axis of the nanomagnet. However, as soon as the magnetization is deflected from the easy axis ($\sin\theta \neq 0$), all the three components of the random field would come into play.

S2 Thermal distributions for θ_{init} and ϕ_{init}

Fig. S1 shows the fluctuations in the polar angle $\theta(t)$ over time due to thermal agitations at 300 K, when the magnetization is nominally along one of two stable orientations along the easy axis ($\theta = 180^\circ$). There is no external torque (e.g., spin-transfer torque) here, but there is a torque due to shape anisotropy since it is a torque internal to the nanomagnet.

In Fig. S1, there are 1 million time steps in the 100 ns interval and this time interval is long enough to make the mean value of $\theta(t)$ independent of the interval duration. Fig. S2 shows the distributions of the polar angle $\theta(t)$ and the azimuthal angle $\phi(t)$ due to thermal fluctuations at 300 K within the same time interval of 100 ns used in Fig. S1. The *most likely* value of θ is 180° which is a stagnation point where spin-transfer-torque vanishes, but the mean value is not 180° . The mean value is $\sim 175.5^\circ$, so that the time-averaged (mean) deviation from the easy axis is $\sim 4.5^\circ$. We noticed that halving the value of M_s does not have any effect on the mean value of θ , or the deviation from the easy axis, because the in-plane shape anisotropy energy barrier is kept constant by adjusting the three components of demagnetization factor. Even though variance of the thermal field $h(t)$ depends on M_s , its mean value is zero, and hence the mean value of the deviation from the easy axis turns out to be relatively independent of M_s . The distribution of $\theta(t)$ appears to be nearly *exponential*, while the distribution of $\phi(t)$ contains two nearly *Gaussian* distributions peaked at the two in-plane angles $\phi = \pm 90^\circ$. Unlike the θ -distribution, the ϕ -distributions are *symmetric* about the mean values.

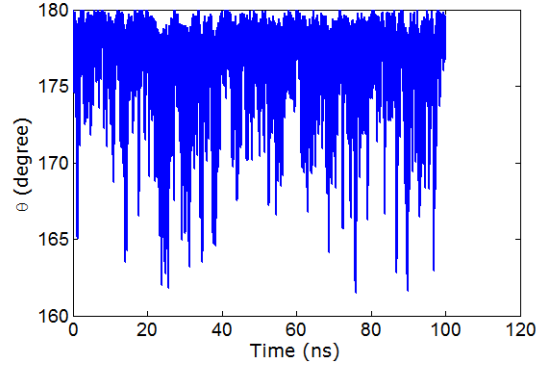


Figure S1: Temporal fluctuations in the polar angle $\theta(t)$ around one of the easy axes ($\theta = 180^\circ$) due to thermal torque at room temperature. The torque due to shape anisotropy is present since it is internal, but there is no spin-transfer-torque which is always applied from an external source. Note that since θ is the polar angle, it is constrained to the interval $[0^\circ, 180^\circ]$. The nanomagnet has saturation magnetization $M_s = 8 \times 10^5$ A/m, the major axis $a = 150$ nm and the minor axis $b = 100$ nm. The in-plane shape anisotropy energy barrier is 0.8 eV or $\sim 32 kT$ at room temperature.

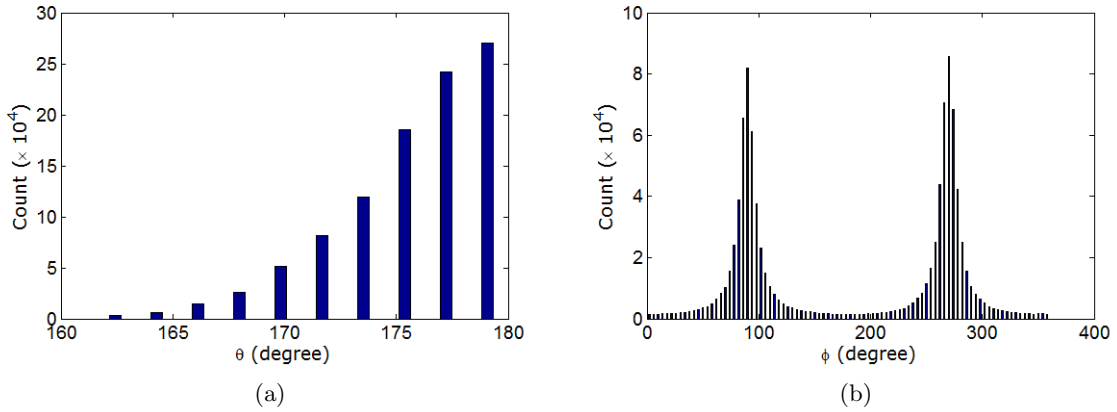


Figure S2: Distributions of the polar angle $\theta(t)$ and azimuthal angle $\phi(t)$ due to thermal fluctuations at room temperature in a nanomagnet of elliptical cross-section. The major axis $a = 150$ nm, the minor axis $b = 100$ nm and the saturation magnetization $M_s = 8 \times 10^5$ A/m. The in-plane shape anisotropy energy barrier is 0.8 eV or $\sim 32 kT$ at room temperature. The magnetization vector is assumed to point in one of two stable orientations along the easy axis ($\theta = 180^\circ$) but is perturbed by thermal fluctuations. (a) Distribution of polar angle $\theta(t)$ due to thermal fluctuations at room temperature. The mean of the distribution is $\sim 175.5^\circ$. (b) Distribution of azimuthal angle $\phi(t)$. There are two peaks in the distribution centered at 90° and 270° (or -90°) that correspond to the plane of the nanomagnet.

S3 Distributions of switching delay and energy dissipation in the presence of thermal fluctuations

Fig. S3 shows the room temperature (300 K) distributions of switching delay and energy dissipation, respectively, when both spin-transfer torque and thermal torque act on a nanomagnet with in-plane shape anisotropy energy barrier of 0.8 eV. The spin-transfer torque is due to an in-plane current of $523 \mu\text{A}$ with 80% spin polarization. The saturation magnetization $M_s = 4.09 \times 10^5 \text{ A/m}$. Here, 10,000 trajectories were simulated to compute these distributions. We assume that when a spin-polarized current is applied to initiate switching, the magnetization vector starts out from near the south pole ($\theta \simeq 180^\circ$) with a certain $(\theta_{init}, \phi_{init})$ picked from the initial angle distributions at 300 K. Switching is deemed to have completed when $\theta(t)$ becomes equal to or less than 4.5° . Note that both distributions are asymmetric about the mean. Regrettably, the long-delay tail extends much farther than the short-delay tail. The high-delay tail is associated with those switching trajectories that start very close to $\theta = 180^\circ$ which is a stagnation point. In such trajectories, the starting torque is vanishingly small, which makes the switching sluggish at the beginning. During this time, switching also becomes susceptible to backtracking because of thermal fluctuations, which increases the delay further. The distribution of energy dissipation is complex, which shows multiple peaks in the distribution. The distribution is due to the variation in internal energy dissipation, E_d (see Fig. 6 in the main paper).

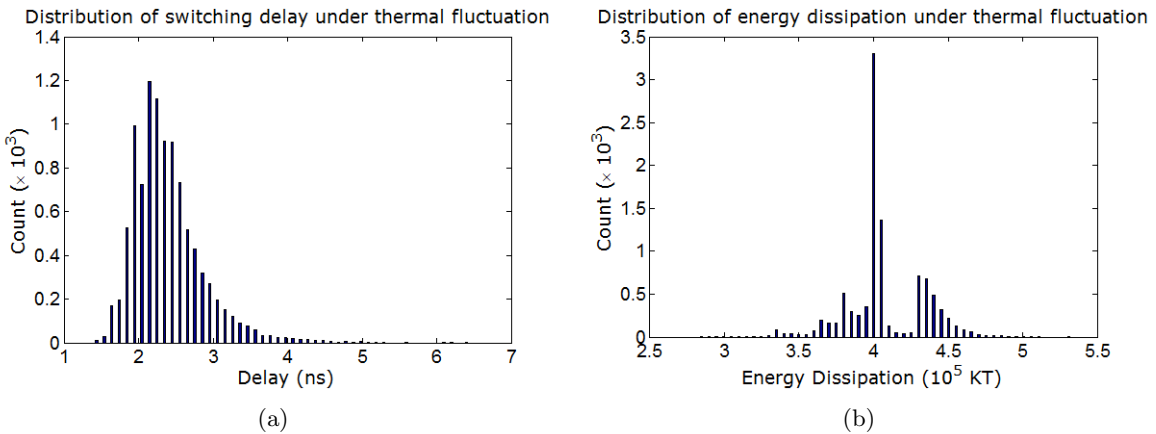


Figure S3: Room temperature (300 K) distributions of switching delay and energy dissipation when a spin-transfer-torque is applied to switch a nanomagnet from one mean thermal deviation from one orientation along the easy axis to one mean thermal deviation from the other diametrically opposite. Here, the saturation magnetization $M_s = 4.09 \times 10^5 \text{ A/m}$ and the in-plane shape anisotropy energy barrier is 0.8 eV. The major axis of the nanomagnet is $a = 300 \text{ nm}$ and the minor axis is $b = 50 \text{ nm}$ to cause this shape anisotropy energy barrier. The magnitude of the in-plane spin-polarized current generating spin-transfer-torque is $523 \mu\text{A}$ and the spin polarization of the current is 80%. (a) Distribution of switching delay: mean value = 2.1 ns, standard deviation = 0.48 ns, and (b) distribution of energy dissipation: mean value = $4.1 \times 10^5 \text{ kT}$ [at room temperature], standard deviation = $2.6 \times 10^4 \text{ kT}$ [at room temperature].

S4 The benefits of switching with a larger switching current I_s

It is obvious that increasing switching current (and hence energy dissipation), while keeping saturation magnetization and shape anisotropy energy barrier constant, will result in faster switching. In order to illustrate this point, we do not consider any thermal fluctuations during the switching to avoid complications; however, the initial orientation of the magnetization is assumed to be $\theta_{init} = 175.5^\circ$ and $\phi_{init} = 90^\circ$ to avoid the stagnation point exactly along the easy axis. Fig. S4 shows the switching dynamics for this case when switching is caused by spin-transfer-torque induced

with an in-plane switching current I_s of 2 mA possessing 80% spin polarization. The saturation magnetization $M_s = 8 \times 10^5$ A/m. The switching occurs in ~ 1 ns, while dissipating 1.25×10^7 kT [$T = 300$ K] of energy. If we increase I_s to 4 mA (Fig. S5) while keeping everything else the same, the switching delay τ drops to 455 ps, but of course the energy dissipation (dominated by $I_s^2 R \tau$) increases by 75%. What Figs. S4 and S5 show is that the reason a higher switching current decreases switching delay is because it suppresses the ripples in the transient dynamics of the magnetization vector. The ripples are caused by complicated precessional motion of the magnetization vector shown in Fig. S4(b). A larger I_s exerts a larger spin-transfer torque on the magnetization vector that suppresses its errant precessional motion and brings about the switching faster. The important point is that since one can always decrease switching current (and hence energy dissipation) by sacrificing switching speed, it is imperative to keep the thermal mean of the switching delay $\langle \tau \rangle$ constant when studying how the switching current I_s scales with saturation magnetization M_s .

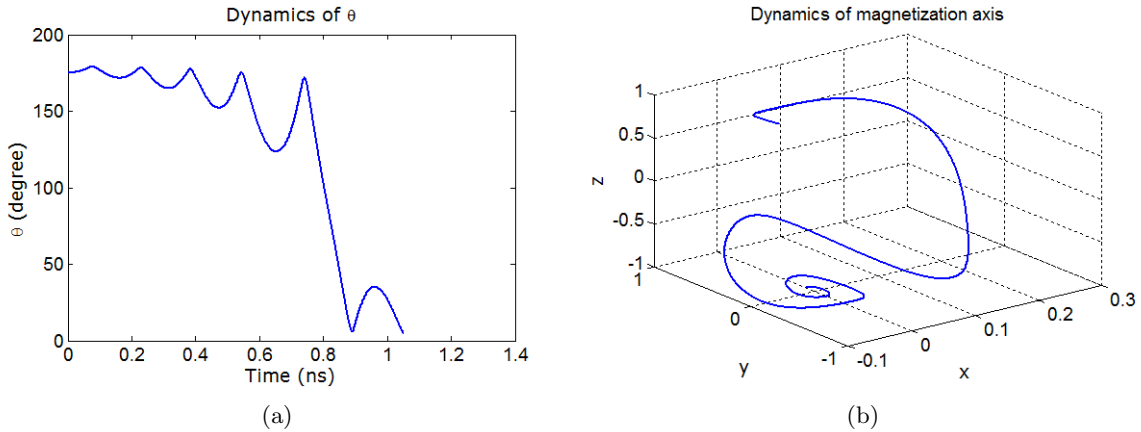


Figure S4: Switching dynamics of the magnetization vector in a nanomagnet of major axis $a = 150$ nm, minor axis $b = 100$ nm, and $M_s = 8 \times 10^5$ A/m, and in-plane shape anisotropy energy barrier of 0.8 eV. This simulation does not consider any thermal fluctuations during the switching, however, the initial orientation of the magnetization is assumed to be $\theta_{init} = 175.5^\circ$ and $\phi_{init} = 90^\circ$ (thermally mean values for 300 K) to avoid the stagnation point exactly along the easy axis. Switching is caused by spin-transfer torque induced with an in-plane current of 2 mA with 80% spin polarization. (a) polar angle $\theta(t)$ versus time, and (b) the trajectory traced out by the tip of the magnetization vector during switching. Switching delay and energy dissipation are 1.05 ns and 1.25×10^7 kT [at room temperature], respectively.

Increasing the switching current, while keeping everything else constant, also decreases the spread (variance) in switching delay caused by thermal fluctuations at non-zero temperatures. Monte Carlo simulations show that the standard deviation in switching delay decreases from 0.23 ns to 0.14 ps at room-temperature when the switching current is increased from 2 mA to 4 mA. This happens because the larger switching current suppresses precessional motion of the magnetization vector that subjects the switching dynamics to greater variability in the presence of thermal fluctuations. A smaller standard deviation in the switching delay helps increasing the operational clock-frequency and facilitates clock synchronization on a chip. Thus, expending more energy to switch (larger I_s) bears some distinct advantages in memory and logic applications, but of course at the cost of increased energy dissipation.

In Fig. S6, we plot the dynamic switching error probability as a function of switching delay τ for different switching currents I_s in the presence of thermal fluctuations at room temperature. Switching *error* occurs when the magnetization vector sets out from its initial stable orientation along the easy axis towards the intended stable orientation diametrically opposite, but fails to reach the latter within the stipulated delay τ because of thermal agitations. For a fixed switching delay, a higher current ensures a higher probability of successful switching because it provides a stronger spin-transfer-torque that overwhelms the thermal torque and suppresses the errant precessional

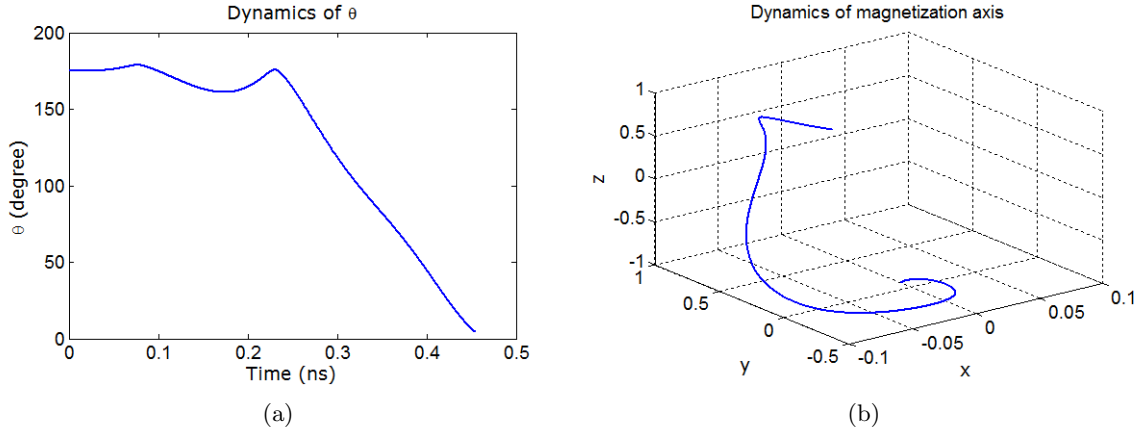


Figure S5: Switching dynamics of the magnetization vector in a nanomagnet of major axis $a = 150$ nm, minor axis $b = 100$ nm, and $M_s = 8 \times 10^5$ A/m. The resulting in-plane shape anisotropy energy barrier is 0.8 eV. This simulation does not consider any thermal fluctuations during the switching, however, the initial orientation of the magnetization is assumed to be $\theta_{init} = 175.5^\circ$ and $\phi_{init} = 90^\circ$ (thermally mean values for 300 K) to avoid the stagnation point exactly along the easy axis. Switching is caused by spin-transfer torque induced with an in-plane current of 4 mA with 80% spin polarization. (a) polar angle $\theta(t)$ versus time, and (b) the trajectory traced out by the tip of the magnetization vector during switching. Switching delay and energy dissipation are 455 ps and $2.2 \times 10^7 kT$ [at room temperature], respectively.

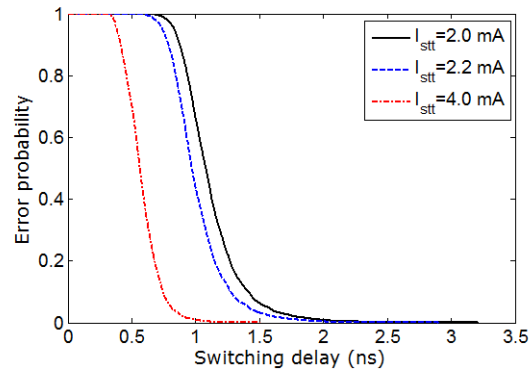


Figure S6: Dynamic switching error probability as a function of switching delay for different switching currents at $T = 300$ K. The nanomagnet has dimensions of $a = 150$ nm, $b = 100$ nm, and the saturation magnetization is $M_s = 8 \times 10^5$ A/m. The resulting in-plane shape anisotropy energy barrier is once again 0.8 eV. Faster switching with a constant current increases the likelihood of error (failure to switch), but at a fixed speed of switching, the error probability decreases with increasing switching current.

motion of the magnetization vector that increases the chances of backtracking and the resulting switching failure. For a fixed switching current, the error probability increases with the speed of switching. This is somewhat obvious; if we allot less time for the switching to complete, it is less likely that switching will complete in that allotted time.

S5 Switching delay-energy as a function of M_s

Fig. S7 shows the switching delay-energy trade-off as a function of saturation magnetization M_s . The plot shows a clear trade-off between the switching delay and energy dissipation as M_s is varied. As M_s is lowered, less energy is dissipated, however, switching delay is increased. The square law scaling of switching current $I_s \propto M_s^2$ is used. As discussed in the main paper, with lower values of M_s , a higher magnitude of current (than that of using the square law $I_s \propto M_s^2$) can reduce the switching delay to some smaller value corresponding to a higher value of M_s , while dissipating lesser energy than that of the high-valued M_s .

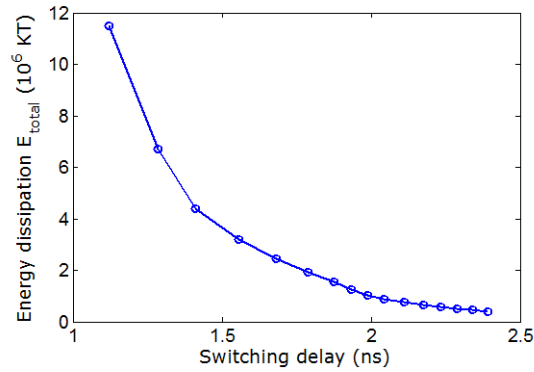


Figure S7: Thermal mean of the total energy dissipation versus thermal mean of the switching delay as a function of saturation magnetization M_s ($4.09 \times 10^5 - 8 \times 10^5$ A/m). The square law scaling of switching current $I_s \propto M_s^2$ is used. A lower M_s incurs less energy dissipation but switching delay is increased.